Continuous and Discontinuous Finite Element Methods for a Peridynamics Model of Mechanics

Xi Chen[1]*and Max Gunzburger[1]

[1] *Department of Scientific Computing, Florida State University, Tallahassee FL 32306-4120, USA*

Abstract. Peridynamics is a recently developed theory of solid mechanics that replaces the partial differential equations (PDE) of classical continuum theories with integro-differential equations (IDE). We apply Finite Element Methods (FEM) as well as Discontinuous Galerkin Methods (DGM) to implement the peridynamic model. Since the integro-differential equations remain valid in the presence of discontinuities such as cracks, it has the potential to model fracture and damage with great generality. We use piecewise constant and discontinuous piecewise linear functions in regions where discontinuities may appear and continuous piecewise linear function in areas where the solutions is smooth and investigate how to combine these two methods. We are also interested in the choice of the horizon radius to implement the peridynamic model more accurately; cases when radius is fixed as a constant or as a function of grid distance are tested. Some theoretical analysis, i.e. existence and uniqueness of the solution and error estimation as well as numerical results for different cases are given.

Key words: peridynamics, discontinuous Galerkin methods, finite element methods

1 Introduction

Nonlocal theories in continuum mechanics have been introduced since at least the 1970s [18,19,25] and have recently become topical again [1–3,7,21,23,24,26,32,33]. The *peridynamics* model [26] is one such nonlocal theory formulated to describe the formation of discontinuities in the displacement field such as cracks and fractures due to deformations. In contrast to the classical local theory and also most other nonlocal approaches, the peridynamic equation of motion is free of any spatial derivatives of displacement. The peridynamic model has been applied in several settings; see, e.g., [4–6,15,16,27–30]. Theoretical studies regarding the peridynamic model are found in, e.g., [9, 10, 12, 17, 26, 31, 34–37]) whereas its computational solution is considered in, e.g., [12,14–16,22,29,35,36]. In particular, finite element discretizations are considered in [14,22,36].

*Corresponding author. *Email addresses:* xc07@fsu.edu (X. Chen), gunzburg@fsu.edu (M. Gunzburger)

In this paper, we study the use of continuous and discontinuous Galerkin finite element methods for discretizing a specific linear peridynamics model. In Section 2, we provide a short overview of bond-based peridynamics models including, in Section 2.2, the specific linearized peridynamics model for proportional microelastic materials. In Section 3, we list the data and exact solutions for the three one-dimensional problems we use to test the accuracy of the discretization methods we develop. Two of these problems have polynomial solutions so that they are smooth whereas the third problem has a solution containing a jump discontinuity. In Section 4, we first provide a variational formulation of a linear, one-dimensional peridynamics model. We then present the three finite element discretization methods we use in our computational studies: continuous piecewise-linear finite element spaces are used in Section 4.1 whereas discontinuous piecewise-constant and piecewise-linear finite element spaces are used in Sections 4.2 and 4.3, respectively. Results of computational experiments for the three test problems and for the three discretization schemes are provided and discussed in Sections 5.1 and 5.2. We compare the relative advantages and disadvantages of the three methods and study the their convergence behaviors. A particular focus of our study is the effects that different choices for the horizon radius, a parameter that appears in the definition of the model, have on the accuracy of the resulting approximations. Then, in Section 5.3, we introduce a hybrid method for which continuous basis functions are used everywhere except in a neighborhood of a jump discontinuity of the solution in which discontinuous basis functions are employed. In Section 6, we provide concluding remarks summarizing our conclusions and describing current and future work. Finally, in Appendix A, we discuss the well-posedness of the variational formulation given in Section 4; in particular, we show that associated bilinear form is continuous and coercive; see also [10, 12, 17, 35, 36].

2 The peridynamics model

2.1 The general bond-based model

We follow the presentation of [26], the paper which introduced the peridynamics model. The acceleration of any particle at $\mathbf{x}$ in the reference configuration at time t is given by

$$\rho\ddot{\mathbf{u}}(\mathbf{x},t) = \int_{H_{\mathbf{x}}} f(\mathbf{u}(\mathbf{x}',t)-\mathbf{u}(\mathbf{x},t),\mathbf{x}'-\mathbf{x})\mathrm{d}V_{\mathbf{x}'}+\mathbf{b}(\mathbf{x},t), \tag{2.1}$$

where $H_{\mathbf{x}}$ denotes a neighborhood of $\mathbf{x}$, $\mathbf{u}$ the displacement vector field, $\mathbf{b}$ a prescribed body force density field, ρ the mass density in the reference configuration, and $\boldsymbol{f}$ a pairwise force function whose value is the force vector (per unit volume squared) that the particle located at $\mathbf{x}'$ (in the reference configuration) exerts on the particle located at the point $\mathbf{x}$ (also in the reference configuration). The relative position $\boldsymbol{\xi}$ of these two particles in the reference configuration is given by

$$\boldsymbol{\xi} = \mathbf{x}'-\mathbf{x}, \tag{2.2}$$

and their relative displacement $\boldsymbol{\eta}$ by

$$\boldsymbol{\eta} = \mathbf{u}(\mathbf{x}',t) - \mathbf{u}(\mathbf{x},t). \tag{2.3}$$

Note that $\boldsymbol{\eta}+\boldsymbol{\xi}$ is the relative position vector between the two particles in the deformed (or current) configuration.

The direct physical interaction between the particles located at $\mathbf{x}$ and $\mathbf{x}'$ is called a bond, or, in the special case of an elastic interaction to be defined below, a spring. The concept of a bond that extends over a finite distance is a fundamental difference between the peridynamic model and classical models for materials which are based on the idea of contact forces, i.e., interactions between particles that are in direct contact with each other.

It is convenient to assume that for a given material there is a positive number δ, called the *horizon*, such that

$$|\boldsymbol{\xi}| > \delta \quad \Rightarrow \quad \mathbf{f}(\boldsymbol{\eta},\boldsymbol{\xi}) = 0 \quad \forall \boldsymbol{\eta} \tag{2.4}$$

which means that the particle $\mathbf{x}$ can not "see" beyond this horizon. In the sequel, we let $H_{\mathbf{x}}$ denote the spherical neighborhood of $\mathbf{x}$ in the body R with radius δ; see Figure 1.

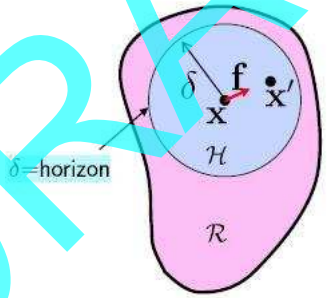

Figure 1: Each point $\mathbf{x}$ in the body interacts directly with points in the sphere $H_{\mathbf{x}}$ through bonds.

The pairwise force function f is required to have the following properties:

$$\mathbf{f}(-\boldsymbol{\eta},-\boldsymbol{\xi}) = -\mathbf{f}(\boldsymbol{\eta},\boldsymbol{\xi}) \quad \forall \boldsymbol{\eta},\boldsymbol{\xi} \tag{2.5}$$

which assures conservation of linear momentum, and

$$(\boldsymbol{\xi}+\boldsymbol{\eta}) \times \mathbf{f}(\boldsymbol{\eta},\boldsymbol{\xi}) = 0 \quad \forall \boldsymbol{\eta},\boldsymbol{\xi} \tag{2.6}$$

which assures conservation of angular momentum. The latter equation means that the force vector between two particles is parallel to their current relative position vector.

2.2 A linearized peridynamics model for microelastic materials

A material is said to be microelastic if the pairwise force function is derivable from a scalar micropotential w:

$$\boldsymbol{f}(\boldsymbol{\eta},\boldsymbol{\xi}) = \frac{\partial w}{\partial \boldsymbol{\eta}}(\boldsymbol{\eta},\boldsymbol{\xi}) \quad \forall \boldsymbol{\eta},\boldsymbol{\xi}. \tag{2.7}$$

The micropotential is the energy in a single bond and has dimensions of energy per unit volume squared. The energy per unit volume in the body at a given point (i.e., the local strain energy density) is therefore found from

$$W = \frac{1}{2}\int_{H_{\mathbf{x}}} w(\boldsymbol{\eta},\boldsymbol{\xi})\mathrm{d}V_{\boldsymbol{\xi}}. \tag{2.8}$$

The factor of $1/2$ appears because each endpoint of a bond "owns" only half the energy in the bond.

If a body is composed of a microelastic material, the work done on it by external forces is stored in a recoverable form in much the same way as in classical theories of elasticity. Furthermore, it can be shown that the micropotential depends on the relative displacement vector $\boldsymbol{\eta}$ only through the scalar distance between the deformed points. Thus, there is a scalar-valued function $\widehat{w}$ such that

$$\widehat{w}(y,\boldsymbol{\xi}) = w(\boldsymbol{\eta},\boldsymbol{\xi}) \quad \forall \boldsymbol{\eta},\boldsymbol{\xi}, \quad y = |\boldsymbol{\eta}+\boldsymbol{\xi}|. \tag{2.9}$$

Therefore, the interaction between any two points in a microelastic material may be thought of as an elastic (and possibly nonlinear) spring. The spring properties may depend on the separation vector $\boldsymbol{\xi}$ in the reference configuration.

A linearized version of the peridynamic model for a microelastic material takes the form

$$\boldsymbol{f}(\boldsymbol{\eta},\boldsymbol{\xi}) = \boldsymbol{C}(\boldsymbol{\xi})\boldsymbol{\eta} \quad \forall \boldsymbol{\eta},\boldsymbol{\xi}, \tag{2.10}$$

where $\boldsymbol{C}$, the micromodulus function for the material, is a second-order tensor given by

$$\boldsymbol{C}(\boldsymbol{\xi}) = \frac{\partial \boldsymbol{f}}{\partial \boldsymbol{\eta}}(\boldsymbol{0},\boldsymbol{\xi}) \quad \forall \boldsymbol{\xi}. \tag{2.11}$$

This function inherits the following requirement from (2.5):

$$\boldsymbol{C}(-\boldsymbol{\xi}) = \boldsymbol{C}(\boldsymbol{\xi}), \quad \forall \boldsymbol{\xi} \tag{2.12}$$

For the special case of proportional materials [11, 13, 26], it follows from (2.10)–(2.12) that

$$\boldsymbol{C}(\boldsymbol{\xi}) = c\frac{\boldsymbol{\xi}\otimes\boldsymbol{\xi}}{|\boldsymbol{\xi}|^3}, \quad \text{i.e.,} \quad C_{ij}(\xi) = c\frac{\xi_i\xi_j}{(\xi_k\xi_k)^{\frac{3}{2}}}, \tag{2.13}$$

where the latter expression uses components in a Cartesian coordinate frame and where c denotes a constant that depends again on the material but also on the dimension of the problem. For example, in one dimension, $c=18k/5\delta^2$, where k denotes the bulk modulus. The determination of c is discussed in detail in [12] and the properties of $\boldsymbol{C}$ are discussed in [26].

Combining (2.1), (2.10), and (2.13), the linearized peridynamic model for a proportional microelastic materials is given by the integro-differential equation

$$\rho\ddot{\mathbf{u}}(\mathbf{x},t)=\int_{H_{\mathbf{x}}} c\frac{(\mathbf{x}'-\mathbf{x})\otimes(\mathbf{x}'-\mathbf{x})}{|\mathbf{x}'-\mathbf{x}|^3}(\mathbf{u}(\mathbf{x}',t)-\mathbf{u}(\mathbf{x},t))\mathrm{d}V_{\mathbf{x}'}+\mathbf{b}(\mathbf{x},t). \tag{2.14}$$

In this paper, we consider the steady-state, one-dimensional model setting for which (2.14), along with a "boundary" condition, reduces to

$$\begin{cases} \dfrac{1}{\delta^2}\displaystyle\int_{x-\delta}^{x+\delta}\frac{u(x)-u(x')}{|x-x'|}\mathrm{d}x'=b(x), & x\in\Omega, \\ \\ u(x)=g(x), & x\in\Gamma, \end{cases} \tag{2.15}$$

where, for convenience, we have set $\rho=1$ and $k=5/18$ and where

$$\Omega=(\alpha,\beta), \qquad \Omega'=(\alpha-\delta,\beta+\delta), \qquad \Gamma=\overline{\Omega'}\setminus\Omega=[\alpha-\delta,\alpha]\cup[\beta,\beta+\delta].$$

The second equation in (2.15) plays a role analogous to that of a Dirichlet boundary condition in classical elasticity, i.e., it fixes the displacement at the "boundary." Because of the nonlocality of the peridynamic model, it is not enough to fix the displacement at the actual domain boundary, but instead the displacement should be fixed along a strip (Γ in (2.15)) along the boundary of thickness given by the horizon δ; see [17, 26].

3 Model problems used in the computational experiments

For the computational experiments, we choose $\alpha=0$ and $\beta=1$ so that $\Omega=(0,1)$ and $\Omega'=(-\delta,1+\delta)$. We also use a uniform grid with spacing $h=2^{-\ell}$ for $\ell=3,\ldots,10$.

We use the method of manufactured solutions to define problems for which we know the exact solution. In some cases, this construction is facilitated by the following observations. If we assume that $u(x)$ is sufficiently smooth and apply Taylor's theorem to the left-hand side of (2.15), we obtain

$$\frac{1}{\delta^2}\int_{x-\delta}^{x+\delta}\frac{u(x)-u(x')}{|x-x'|}\mathrm{d}x'=-\frac{1}{2}u''(x)-\frac{1}{48}u''''(x)\delta^2+\cdots \tag{3.1}$$

which we can use to determine the right-hand side $b(x)$ of (2.15) for polynomial exact solutions $u(x)$. For example, from (3.1),

$$\text{for} \quad u(x)=x(1-x), \quad \text{we have} \quad b(x)=1 \tag{3.2}$$

and

$$\text{for} \quad u(x)=x^2(1-x^2), \quad \text{we have} \quad b(x)=6x^2+\tfrac{1}{2}\delta^2-1. \tag{3.3}$$

Note that unlike the right-hand side corresponding to the exact solution given in (3.2), the one given in (3.3) depends on the horizon δ.

The exact solutions given in (3.2) and (3.3) are smooth and, of course, it is important to test a discretization method for the peridynamic model for such solutions. However, we also want to test discretization methods for problems with discontinuous solutions because one of the strengths of the peridynamic model is that it does not involve spatial derivatives so that is allows for solutions with jump discontinuities. Thus, we also test discretization methods for the exact solution

$$u(x)=\begin{cases} x & \text{for } x<0.5 \\ x^2 & \text{for } x>0.5 \end{cases} \tag{3.4}$$

shown in Figure 2 (left). Of course, we cannot use (3.1) to determine the corresponding right-hand side $b(x)$, so, by direct substitution, we determine it to be

$$b(x)=\begin{cases} 0 & \text{for } x\in[0,0.5-\delta) \\ \frac{1}{2}\delta^2-\delta+\frac{3}{8}+(2\delta-\frac{3}{2}-\ln\delta)x & \\ \qquad +(\frac{3}{2}+\ln\delta)x^2-(x^2-x)\ln(\frac{1}{2}-x) & \text{for } x\in[0.5-\delta,0.5) \\ \frac{1}{2}\delta^2-\delta+\frac{3}{8}+(2\delta+\frac{3}{2}+\ln\delta)x & \\ \qquad -(\frac{3}{2}+\ln\delta)x^2+(x^2-x)\ln(x-\frac{1}{2}) & \text{for } x\in(0.5,0.5+\delta) \\ 1 & \text{for } x\in[0.5+\delta,1.0]. \end{cases}$$

For $\delta=0.3$, a plot of this function is given Figure in 2 (right).

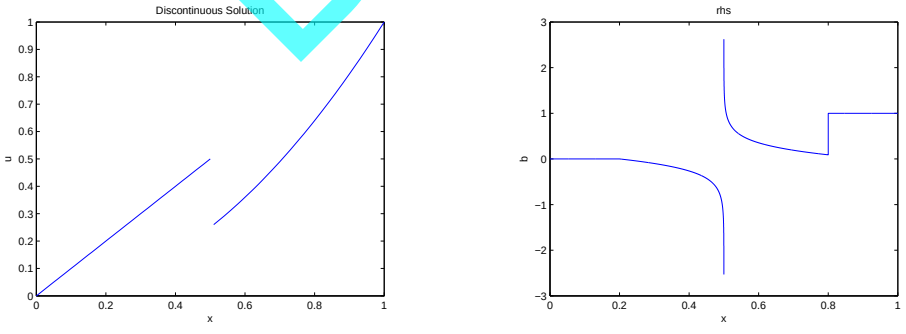

Figure 2: Left: the discontinuous solution (3.4); right: the corresponding forcing function $b(x)$.

4 Galerkin finite element discretization

Define the affine space $S_g = \{u(x) \in L_2(\Omega') \mid u(x) = g(x) \text{ a.e. on } \Gamma\}$ and the space $S_0 = \{v(x) \in L_2(\Omega') \mid v(x) = 0 \text{ on } \Gamma\}$ and denote the inner product on $L^2(\Omega)$ by $\big(u(x),v(x)\big) = \int_\alpha^\beta u(x)v(x)\mathrm{d}x$. Then, a variational formulation for (2.15) is given by

$$\begin{cases} \text{given } b(x) \in L^2(\Omega) \text{ and } g(x) \in L^2(\Gamma), \text{ seek } u(x) \in S_g \text{ satisfying} \\ \\ \dfrac{1}{\delta^2}\Big(\displaystyle\int_{x-\delta}^{x+\delta} \frac{u(x)-u(x')}{|x-x'|}\mathrm{d}x' \,,\, v(x)\Big) = \Big(b(x)\,,\,v(x)\Big) \quad \forall v(x) \in S_0 \end{cases} \tag{4.1}$$

Let $S^h \subset L^2(\Omega')$ denote a family of finite-dimensional subspaces parameterized by a parameter h. For $x \in \Gamma$, let $g^h(x)$ denote an approximation of $g(x)$; if $g(x)$ is sufficiently smooth, we can choose $g^h(x) \in S^h|_\Gamma$ to be an interpolant of $g(x)$; otherwise, we can choose $g^h(x) \in S^h|_\Gamma$ to be the $L^2(\Gamma)$ projection of $g(x)$. We then define the affine space $S_g^h = \{u^h(x) \in S^h \mid u^h(x) = g^h(x) \text{ a.e. on } \Gamma\}$ and the subspace $S_0^h = \{v^h \in S^h \mid v^h = 0 \text{ on } \Gamma\} \subset S_0$. Then, the Galerkin approximation to (4.1) is given by

$$\begin{cases} \text{given } b(x) \in L^2(\Omega) \text{ and } g^h(x) \in S_0^h, \text{ seek } u^h(x) \in S_g^h \text{ satisfying} \\ \\ \dfrac{1}{\delta^2}\Big(\displaystyle\int_{x-\delta}^{x+\delta} \frac{u^h(x)-u^h(x')}{|x-x'|}\mathrm{d}x', v^h(x)\Big) = \Big(b(x), v^h(x)\Big) \quad \forall v^h(x) \in S_0^h. \end{cases} \tag{4.2}$$

Define a partition of $\Omega' = [\alpha-\delta,\beta+\delta]$ such that $x = \alpha-\delta$, α, β, and $\beta+\delta$ are all nodes of the partition, i.e., we have, for given positive integers K and N,

$$\alpha-\delta = x_{-K} < \cdots < x_{-1} < \alpha = x_0 < x_1 < \cdots < x_N < x_{N+1} = \beta < x_{N+2} < \ldots < x_{N+K+1} = \beta+\delta. \tag{4.3}$$

Then h denotes the maximum length of any of the subintervals (x_j,x_{j+1}), $j = -K,\ldots,K+N$.

4.1 Continuous piecewise-linear finite element spaces

We choose S^h to be the space of continuous piecewise-linear polynomials defined with respect to the partition (4.3). We also choose the standard "hat" functions as a basis $\{\phi_j(x)\}_{j=-K}^{N+K+1}$ for S^h.

Let $u^h(x) = \sum_{j=-K}^{N+K+1} u_j\phi_j(x)$ and, for $i = 1,\ldots,N$, let $v^h(x) = \phi_i(x)$. Then, (4.2) is equivalent to

$$\frac{1}{\delta^2}\sum_{j=-K}^{N+K+1} u_j\Big(\int_{x-\delta}^{x+\delta} \frac{\phi_j(x)-\phi_j(x')}{|x-x'|}\mathrm{d}x', \phi_i(x)\Big) = \Big(b(x),\phi_i(x)\Big) \quad \text{for } i = 1,\ldots,N, \tag{4.4}$$

where $u_j = g^h(x_j)$ for $j = -K,\ldots,0$ and $j = N+1,\ldots,N+K+1$. Because $g^h(x)$ is determined (by interpolation or projection) from the "boundary" data $g(x)$, these coefficients are determined from that data; in particular, if it is possible to use the $S^h|_\Gamma$ interpolant, we have

$u_j = g(x_j)$ for the indicated values of j. Let the entries of the $N \times N$ matrix $\mathbb{A}$ be defined by

$$\mathbb{A}_{ij} = \frac{1}{\delta^2}\Big(\int_{x-\delta}^{x+\delta} \frac{\phi_j(x)-\phi_j(x')}{|x-x'|}\mathrm{d}x', \phi_i(x)\Big) \quad \text{for } i,j=1,\ldots,N \tag{4.5}$$

and let the components of the N-vector $\mathbf{b}$ be defined by

$$\begin{aligned}\mathbf{b}_i = \Big(b(x),\phi_i(x)\Big) &- \sum_{j=-K}^{0} g_h(x_j)\Big(\int_{x-\delta}^{x+\delta} \frac{\phi_j(x)-\phi_j(x')}{|x-x'|}\mathrm{d}x', \phi_i(x)\Big) \\ &- \sum_{j=N+1}^{N+K+1} g_h(x_j)\Big(\int_{x-\delta}^{x+\delta} \frac{\phi_j(x)-\phi_j(x')}{|x-x'|}\mathrm{d}x', \phi_i(x)\Big) \quad \text{for } i=1,\ldots,N.\end{aligned} \tag{4.6}$$

Also, let the entries of the N-vector $\mathbf{U}$ of unknown coefficients be defined by $\mathbf{U}_j = u_j$ for $j=1,\ldots,N$. Then, the linear system (4.4) can be expressed in the form

$$\mathbb{A}\mathbf{U} = \mathbf{b}. \tag{4.7}$$

From the results given in Appendix A, it is easily shown that the matrix $\mathbb{A}$ is symmetric and positive definite so that the linear system (4.7), or equivalently, (4.4), has a unique solution which implies that the finite element approximation $u^h(x)$ determined from (4.2) is uniquely defined.

Due to the nonlocality of the peridynamic model, the matrix $\mathbb{A}$ is, in general, not tridiagonal, even though the basis functions are the piecewise linear hat functions. The right-hand side of (4.5) is a double integral, i.e., we have

$$\mathbb{A}_{ij} = \frac{1}{\delta^2}\int_{x_{i-1}}^{x_{i+1}} \phi_i(x) \int_{x-\delta}^{x+\delta} \frac{\phi_j(x)-\phi_j(x')}{|x-x'|}\mathrm{d}x'\mathrm{d}x \quad \text{for } i,j=1,\ldots,N, \tag{4.8}$$

where we have used the fact that the basis functions $\phi_i(x)$ has support on the interval (x_{i-1},x_{i+1}), i.e., $\phi_i(x)=0$ whenever $x \notin (x_{i-1},x_{i+1})$. We also have that

$$\int_{x-\delta}^{x+\delta} \frac{\phi_j(x')}{|x-x'|}\mathrm{d}x' \neq 0 \quad \text{for all } j \text{ such that} \quad \mathrm{supp}\{\phi_j(x')\} \in (x-\delta,x+\delta).$$

Suppose the partition (4.3) is uniform so that $x_j = jh$ for $j=-K,\ldots,N+K+1$ and suppose $\delta > h$. Then, we have that $(x_j,x_{j+1}) \subset (x-\delta,x+\delta)$ so that for $j=i+2$ and perhaps for larger j, we have that $\mathbb{A}_{ij} \neq 0$ and likewise for $j=i-2$ and perhaps for smaller j. For example, if we choose δ such that $\delta = Mh$ for a fixed integer M, we have that

$$\mathbb{A}_{ij}=0 \quad \text{if} \quad j > i+M+1 \text{ or } j < i-M-1 \qquad \text{and} \qquad \mathbb{A}_{ij} \neq 0 \quad \text{if} \quad i-M-1 \leq j \leq i+M+1,$$

so that $\mathbb{A}$ is a banded matrix with fixed upper and lower half-bandwidth $M+1$ for any h. On the other hand, if the horizon δ is fixed independent of h, then the half-bandwidths increase as h decreases. For example, if we choose a sequence of decreasing grid spacings

$h=\delta/m$ with δ independent of h and m an increasing sequence of integers, then the half-bandwidths increase linearly with m.

In general, both the inner and outer integrals in (4.8) have to be approximated by quadrature rules. If one applies a quadrature rule defined with respect to the interval $(x-\delta,x+\delta)$ to the inner integral, it is possible, because of the denominator $|x-x'|$, that the integrand is singular at one of the quadrature points. To guarantee that this does not occur, e.g., for the diagonal entries $\mathbb{A}_{jj}$, we split the double integral into 8 terms:

$$\begin{aligned}
\delta^2 A_{jj} &= \int_{x_{j-1}}^{x_{j+1}} \phi_j(x) \int_{x-\delta}^{x+\delta} \frac{\phi_j(x)-\phi_j(x')}{|x-x'|}\mathrm{d}x'\mathrm{d}x \\
&= \int_{x_{j-1}}^{x_j} {\phi_j}^2(x) \int_{x-\delta}^{x_{j-1}} \frac{1}{x-x'}\mathrm{d}x'\mathrm{d}x + \int_{x_{j-1}}^{x_j} \phi_j(x) \int_{x_{j-1}}^{x} \frac{\phi_j(x)-\phi_j(x')}{x-x'}\mathrm{d}x'\mathrm{d}x \\
&\quad + \int_{x_{j-1}}^{x_j} \phi_j(x) \int_{x}^{x_j} \frac{\phi_j(x)-\phi_j(x')}{x'-x}\mathrm{d}x'\mathrm{d}x + \int_{x_{j-1}}^{x_j} \phi_j(x) \int_{x_j}^{x+\delta} \frac{\phi_j(x)-\phi_j(x')}{x'-x}\mathrm{d}x'\mathrm{d}x \\
&\quad + \int_{x_j}^{x_{j+1}} \phi_j(x) \int_{x-\delta}^{x_j} \frac{\phi_j(x)-\phi_j(x')}{x-x'}\mathrm{d}x'\mathrm{d}x + \int_{x_j}^{x_{j+1}} \phi_j(x) \int_{x_j}^{x} \frac{\phi_j(x)-\phi_j(x')}{x-x'}\mathrm{d}x'\mathrm{d}x \\
&\quad + \int_{x_j}^{x_{j+1}} \phi_j(x) \int_{x}^{x_{j+1}} \frac{\phi_j(x)-\phi_j(x')}{x'-x}\mathrm{d}x'\mathrm{d}x + \int_{x_j}^{x_{j+1}} {\phi_j}^2(x) \int_{x_{j+1}}^{x+\delta} \frac{1}{x'-x}\mathrm{d}x'\mathrm{d}x.
\end{aligned}$$

Then, if we use Gauss quadrature rules to approximate each of the outer and inner integrals, we avoid the possibility of the integrand being singular. A similar splitting, with fewer terms, is done for the off-diagonal entries.

4.2 Discontinuous piecewise-constant finite element spaces

The peridynamic model does not contain spatial derivatives of the solution so that finite element spaces consisting of functions with jump discontinuities are *conforming* for the variational formulation of the peridynamic model. Thus, we also consider such discontinuous finite element spaces for obtaining approximate solutions of the peridynamic model.

We again use the uniform partition of Ω' defined in (4.3). Then, the simplest choice of basis functions for discontinuous Galerkin methods are the piecewise constants, i.e.,

$$\phi_j(x) = \begin{cases} 1 & \text{for } x \in (x_{j-1},x_j) \\ 0 & \text{otherwise} \end{cases} \qquad \text{for } j=-K+1,\ldots,K+N+1.$$

Through the same process as for the continuous piecewise linear functions, we are led to a linear system of the type (4.7), where now $\mathbb{A}$ is an $(N+1)\times(N+1)$ matrix and $\mathbf{U}$ and $\mathbf{b}$

are $(N+1)$-vectors. The diagonal entries of the matrix $\mathbb{A}$ are now given by

$$\begin{aligned}\delta^2\mathbb{A}_{ii} = \int_{x_{i-1}}^{x_i}\int_{x-\delta}^{x+\delta}\frac{\phi_i(x)-\phi_i(x')}{|x-x'|}\mathrm{d}x'\mathrm{d}x = \int_{x_{i-1}}^{x_i}\int_{x-\delta}^{x+\delta}\frac{1}{|x-x'|}\mathrm{d}x'\mathrm{d}x \\ -\int_{x_{i-1}}^{x_i}\int_{\max(x_{i-1},x-\delta)}^{\min(x_i,x+\delta)}\frac{1}{|x-x'|}\mathrm{d}x'\mathrm{d}x \qquad \text{for } i=1,\ldots,N+1,\end{aligned} \tag{4.9}$$

where we have used the fact that $\phi_i(x)=1$ within its support interval (x_{i-1},x_i) and vanishes elsewhere. The off-diagonal entries are given by, as long as $\max(x_{j-1},x-\delta) < \min(x_j,x+\delta)$,

$$\delta^2\mathbb{A}_{ij} = -\int_{x_{i-1}}^{x_i}\int_{\max(x_{j-1},x-\delta)}^{\min(x_j,x+\delta)}\frac{1}{|x-x'|}\mathrm{d}x'\mathrm{d}x \quad \text{for } i,j=1,\ldots,N+1,\ j\neq i, \tag{4.10}$$

where we have also used the facts that $\phi_j(x)=0$ for $x\in(x_{i-1},x_i)$ when $j\neq i$ and that $\phi_j(x')=1$ within its support interval (x_{j-1},x_j) and vanishes elsewhere. If $\max(x_{j-1},x-\delta)\geq\min(x_j,x+\delta)$, we have that $\mathbb{A}_{ij}=0$. Clearly, $\mathbb{A}$ is a banded matrix and again, if δ is fixed independent of h, the bandwidth increases as h is decreases, whereas, if δ is a multiple of h, the bandwidth remains fixed as h is decreases.

An important observation about discontinuous Galerkin methods for the peridynamic model is that, unlike the case for the applications of such methods to elliptic partial differential equation problems, *there is no need to include "jump" terms that explicitly account for the continuity of fluxes across element boundaries.* Of course, this is a result of the fact that discontinuous finite element spaces are conforming for the variational formulation of the peridynamic model.

4.3 Discontinuous piecewise-linear finite element spaces

Once again we use the uniform partition of Ω' defined in (4.3). A basis for the space of discontinuous piecewise-linear discontinuous basis function is given by

$$\phi_{2j}(x) = \begin{cases} \dfrac{x_j-x}{x_j-x_{j-1}} & \text{for } x\in(x_{j-1},x_j) \\ 0 & \text{otherwise}\end{cases}$$

and

$$\phi_{2j+1}(x) = \begin{cases} \dfrac{x-x_{j-1}}{x_j-x_{j-1}} & \text{for } x\in(x_{j-1},x_j) \\ 0 & \text{otherwise}\end{cases}$$

for $j=-K+1,\ldots,K+N+1$. Now $\mathbb{A}$ is an $(2N+2)\times(2N+2)$ matrix and $\mathbf{U}$ and $\mathbf{b}$ are $(2N+2)$-vectors. For the sake of brevity, we do not write down formulas for the entries of the matrix $\mathbb{A}$.

An important observation is that *the space of* discontinuous *piecewise-linear functions contains the space of* continuous *piecewise-linear functions.* Obviously, the same cannot be said for the space of discontinuous piecewise-constant functions.

5 Computational results

We present results of computational experiments for each of the model problems having solutions (3.2)–(3.4) and for each of the three discretization schemes discussed in Sections 4.1–4.3. Moreover, we examine both the case for which the horizon δ depends on the grid spacing h and when it is fixed independent of h. Note that in [26], it is recommended to choose the horizon $\delta = 3h$ so that the horizon depends on the grid spacing. One advantage of such a choice is that the bandwidth of the matrix $\mathbb{A}$ remains fixed as h decreases.

We note that the computational results present here for the discontinuous exact solution (3.4) use a "best-case scenario' in the sense that we place a grid point exactly at the location of the point of discontinuity of the solution. We see that even in this case, there are significant differences in the performance of the different finite element methods we test. In practice, it may not be possible to determine the exact location of the points or surfaces of discontinuity in a solution; in such cases, it may be necessary to appropriately refine the grid near such points in order to obtain the levels of accuracy attainable when one knows the exact locations of discontinuities. An adaptive strategy can be easily defined to determine the regions in which such grid refinement are needed.[†]

We will draw several *tentative* conclusions from the computational results. Of course, many more extensive computational studies and numerical analyses need be done, especially in two and three dimensions and for nonlinear problems, before these conclusions can be made more definitive.

5.1 Continuous piecewise-linear finite elements

We begin with the continuous piecewise-linear finite element discretization discussed in Section 4.1.

Smooth exact solutions with horizon dependent on the grid size. Following the suggestion made in [26], we first examine the convergence of the continuous piecewise-linear finite element approximation in case the horizon δ is chosen proportional to the grid size h. Specifically, for the exact solution given in (3.2), we present, in Table 1, results for $\delta = 3h$ and, in Figure 3, results for $\delta = 2h$, $3h$, and $4h$. In the table and figure, we provide the $L^2(\Omega)$ and $L^\infty(\Omega)$ norms and the $H^1(\Omega)$ semi-norms of the error for a sequence of grid sizes and the corresponding rates of convergence. Similar information is provided in Table 2 and Figure 3 for the exact solution given in (3.3).

Smooth exact solutions with horizon fixed independent of the grid size. If one takes the view that the horizon δ is a material parameter, then its value should not depend on any discretization parameter, including the grid size h. Thus, we also examine errors and

[†]In [6], effective adaptive grid refinement strategies are discussed for a discretization of (2.15) through a midpoint quadrature rule approximation of the integral appearing on the left-hand side.

convergence rates for cases in which the value of the horizon δ is fixed independent of h. Recall that, in this case, the bandwidth of the matrix $\mathbb{A}$ increases as h decreases. Results are provided for the exact solutions given in (3.2) and (3.3) in Tables 3 and 4 for $\delta = 0.001$ and in Figure 4 for $\delta = 0.1$, 0.01, and 0.001. Note that $h < \delta$ for some values of h and $h > \delta$ for others.

Discontinuous exact solutions with horizon dependent on the grid size. We next examine the convergence of continuous piecewise-linear finite element discretizations for the problem having the exact solution given in (3.4) that has a jump discontinuity. We first consider, as we did for the continuous exact solution experiments, the case of the horizon δ being proportional to the grid size h. Results are provided on the left of Table 5 and in Figure 5. Errors with respect to the H^1-semi norm are not provided because the exact solution does not belong to $H^1(\Omega)$.

Discontinuous exact solutions with horizon fixed independent of the grid size. Next, we consider the same case as that of the previous paragraph, but now we keep the value of the horizon δ fixed independent of the grid size h. Results are provided on the right of Table 5 and in Figure 5. Again, errors with respect to the H^1-semi norm are not provided because the exact solution does not belong to $H^1(\Omega)$.

5.1.1 Discussion

Based on the results presented in Tables 1–5 and Figures 3–5, we make the following observations.

- For smooth solutions such as the ones given in (3.2) and (3.3), continuous piecewise-linear finite element approximations of the linear peridynamic model (2.15) converge at the optimal rates, i.e., the L^2 and L^∞ errors are of roughly order $O(h^2)$ and the H^1 errors are of roughly order $O(h)$. This statement is true both if the horizon δ is chosen proportional to the grid size h or if it is chosen fixed independent of h. In the case for which δ is fixed, the optimal convergence rates are attained for both $\delta < h$ and $\delta > h$.

- For smooth solutions, the rates of convergence attained by continuous piecewise-linear finite element approximations of the linear peridynamic model are the same as those obtained from the analogous finite element discretization of linear classical elastic models.

- For solutions containing jump discontinuities such as the one given in (3.4), continuous piecewise-linear finite element approximations of the linear peridynamic model (2.15) are seriously compromised, even though we are placing a grid point exactly at the point of discontinuity of the exact solution. The L^2 errors are of $O(h^{1/2})$ and there is no convergence with respect to the L^∞ norm. This statement is

true both if the horizon δ is chosen proportional to the grid size h or if it is chosen fixed independent of h.

- For solutions with jump discontinuities, the L^2 rate of convergence is optimal, given that the exact solution belongs to $H^{1/2-\epsilon}(\Omega)$ for any $\epsilon > 0$, but is no smoother than that. This is also the rate obtained from the analogous finite element discretization of linear classical elastic models.

The fact that, for smooth solutions, optimally accurate approximations are obtained even for $\delta < h$ is noteworthy. For such δ, the peridynamic model essentially becomes a local model so that one sees that smooth solutions are basically obtainable from local models. Thus, for such solutions, one may as well use classical elastic models. From the accuracy point of view, there also seems to be little advantage, relative to classical elastic models, to using the peridynammics model for problems with smooth solutions. Another interpretation of fact that, for smooth solutions, optimally accurate solutions are obtained for any choice of δ is that, in such a case, δ should not be interpreted as being a material parameter and thus can be chosen for convenience, e.g., to minimize bandwidth or to simplify the coupling of the continuum peridynamic model to atomistic models.

For solutions containing jump discontinuities, the use of *continuous* piecewise-linear finite element discretizations of the linear peridynamic model also offers no advantage over using the same type of discretization for classical elastic models. For both models, the approximations are similarly compromised.

We note that, at least with respect to the $L^2(\Omega)$ norm, the rates of convergence given in the tables and figures[‡] for the cases for which the horizon δ is chosen independent of the grid size h should be provable. In Appendix A, it is shown that the bilinear form associated with the variational formulation (4.1) is continuous and coercive with respect to the peridynamic "energy" norm defined in (A.1). Further, in [10], it is further shown that, for the particular linear peridynamic model considered here, that norm is equivalent to the $L^2(\Omega)$ norm. Then, standard finite element analyses should yield, for continuous piecewise linear-approximations,

$$\|u - u^h\|_{L^2(\Omega)} \leq C h^{\min\{s,2\}} \|u\|_{H^s(\Omega)}, \tag{5.1}$$

where $H^s(\Omega)$ denotes the standard Sobolev space. For the exact solutions given in (3.2) and (3.3), we have that $\min\{s,2\} = 2$ whereas for the exact solution given in (3.4), we have $\min\{s,2\} = \frac{1}{2} - \epsilon$. The rates of convergence given in the appropriate tables and figures are entirely consistent with this estimate.

[‡]See Tables 3, 4, and the table on the right in Table 5 and Figure 4 and the plot on the right of Figure 5.

Table 1: Errors and convergence rates of continuous piecewise-linear approximations for $\delta = 3h$ for the *smooth* exact solution (3.2).

	L^2		L^∞		H^1	
h	Error	Rate	Error	Rate	Error	Rate
2^{-3}	2.50E-3	–	3.90E-3	–	6.25E-2	–
2^{-4}	6.67E-4	1.91	9.76E-4	2.00	3.38E-2	0.89
2^{-5}	1.73E-4	1.95	2.44E-4	2.00	1.75E-2	0.95
2^{-6}	4.38E-5	1.98	6.10E-5	2.00	8.90E-3	0.98
2^{-7}	1.10E-5	1.99	1.52E-5	2.00	4.50E-3	0.98
2^{-8}	2.70E-6	2.00	3.81E-6	2.00	2.20E-3	1.03
2^{-9}	6.26E-7	2.01	9.52E-7	2.00	1.10E-3	1.00
2^{-10}	1.13E-7	2.03	2.38E-7	2.00	5.63E-4	0.97

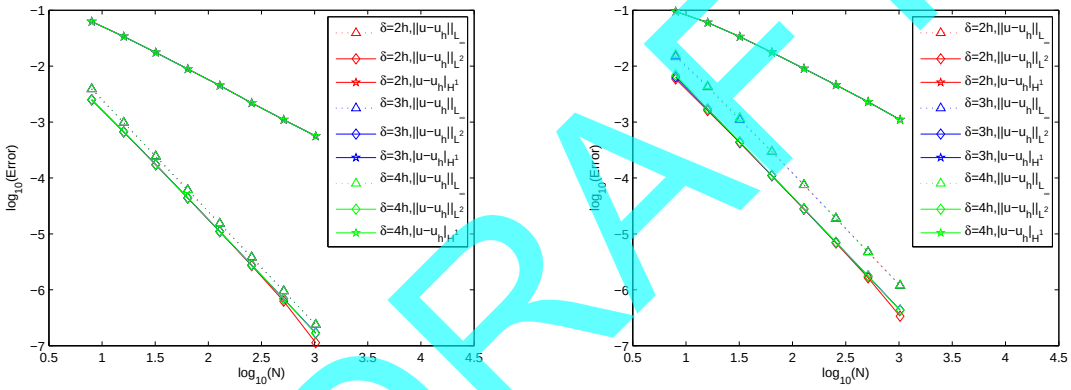

Figure 3: L^2, L^∞, and H^1 errors vs. $N = 1/h$ for continuous piecewise linear approximations for $\delta = 2h$, $3h$, and $4h$, left: exact solution (3.2); right: exact solution (3.3).

Table 2: Errors and convergence rates of continuous piecewise-linear approximations for $\delta = 3h$ for the *smooth* exact solution (3.3).

	L^2		L^∞		H^1	
h	Error	Rate	Error	Rate	Error	Rate
2^{-3}	6.40E-3	–	1.52E-2	–	9.51E-2	–
2^{-4}	1.70E-3	1.91	4.30E-3	1.82	6.02E-2	0.66
2^{-5}	4.36E-4	1.96	1.10E-3	1.97	3.35E-2	0.85
2^{-6}	1.11E-4	1.97	2.96E-4	1.89	1.76E-2	0.93
2^{-7}	2.80E-5	1.99	7.51E-5	1.98	9.00E-3	0.98
2^{-8}	7.03E-6	1.99	1.89E-5	1.99	4.60E-3	0.97
2^{-9}	1.76E-6	2.00	4.75E-6	1.99	2.30E-3	1.00
2^{-10}	4.34E-7	2.02	1.19E-6	2.00	1.10E-3	1.06

Table 3: Errors and convergence rates of continuous piecewise-linear approximations for $\delta = 0.001$ for the *smooth* exact solution (3.2).

	L^2		L^∞		H^1	
h	Error	Rate	Error	Rate	Error	Rate
2^{-3}	2.50E-3	–	4.00E-3	–	6.25E-2	–
2^{-4}	6.59E-4	1.92	9.72E-4	2.04	3.38E-2	0.89
2^{-5}	1.71E-4	1.95	2.44E-4	2.00	1.75E-2	0.95
2^{-6}	4.32E-5	1.98	6.09E-5	2.00	8.90E-3	0.98
2^{-7}	1.11E-5	1.96	1.54E-5	1.99	4.50E-3	0.98
2^{-8}	2.80E-6	1.99	3.85E-6	2.00	2.20E-3	1.03
2^{-9}	7.01E-7	1.98	9.74E-7	1.98	1.10E-3	1.00
2^{-10}	1.75E-7	2.02	2.37E-7	2.04	5.63E-4	0.97

Table 4: Errors and convergence rates of continuous piecewise-linear approximations for $\delta = 0.001$ for the *smooth* exact solution (3.3).

	L^2		L^∞		H^1	
h	Error	Rate	Error	Rate	Error	Rate
2^{-3}	3.90E-3	–	1.18E-2	–	9.50E-2	–
2^{-4}	1.30E-3	1.70	3.80E-3	1.63	6.02E-2	0.66
2^{-5}	3.28E-4	1.87	1.10E-3	1.79	3.35E-2	0.85
2^{-6}	8.76E-5	1.90	2.88E-4	1.93	1.76E-2	0.93
2^{-7}	2.31E-5	1.92	7.43E-5	1.96	9.00E-3	0.97
2^{-8}	6.01E-6	1.94	1.88E-5	1.98	4.60E-3	0.97
2^{-9}	1.60E-6	1.91	4.78E-6	1.99	2.30E-3	1.00
2^{-10}	3.77E-7	2.09	1.18E-6	2.01	1.20E-3	0.94

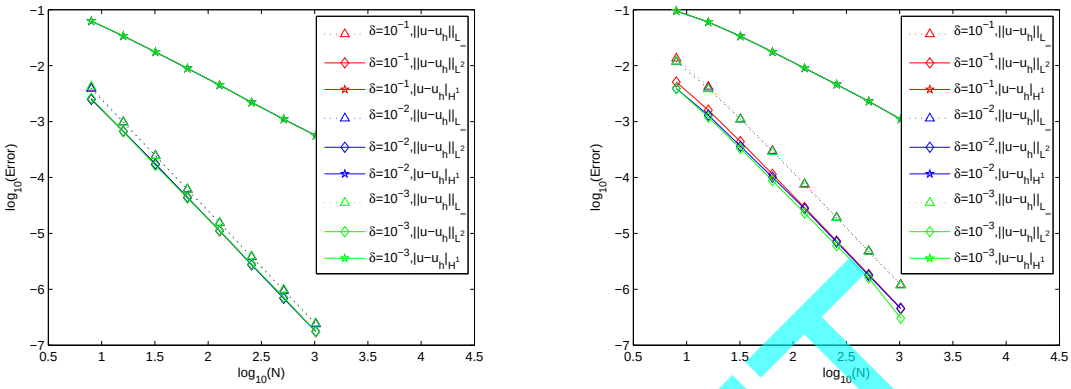

Figure 4: L^2, L^∞, and H^1 errors vs. $N=1/h$ for continuous piecewise linear approximations for $\delta=0.1$, 0.01, and 0.001, left: exact solution (3.2); right: exact solution (3.3).

Table 5: Errors and convergence rates of continuous piecewise-linear approximations for the *discontinuous* exact solution (3.4).

	$\delta=3h$				$\delta=0.001$			
	L^2		L^∞		L^2		L^∞	
h	Error	Rate	Error	Rate	Error	Rate	Error	Rate
2^{-3}	3.40E-2	–	1.25E-1	–	3.68E-2	–	1.25E-1	–
2^{-4}	2.38E-2	0.52	1.25E-1	0	2.56E-2	0.52	1.25E-1	0
2^{-5}	1.68E-2	0.52	1.25E-1	0	1.80E-2	0.51	1.25E-1	0
2^{-6}	1.19E-2	0.50	1.25E-1	0	1.27E-2	0.50	1.25E-1	0
2^{-7}	0.84E-2	0.50	1.25E-1	0	0.90E-2	0.50	1.25E-1	0
2^{-8}	0.59E-2	0.50	1.25E-1	0	0.63E-2	0.52	1.25E-1	0
2^{-9}	0.42E-2	0.49	1.25E-1	0	0.44E-2	0.52	1.25E-1	0
2^{-10}	0.30E-2	0.49	1.25E-1	0	0.30E-2	0.55	1.25E-1	0

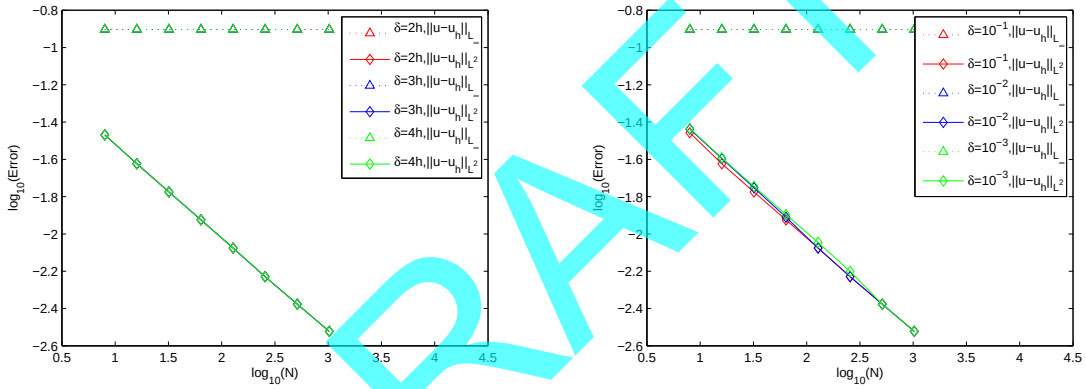

Figure 5: L^2 and L^∞ errors vs. $N = 1/h$ for continuous piecewise linear approximations for the *discontinuous* exact solution (3.4); left: $\delta = 2h$, $3h$, and $4h$; right: $\delta = 0.1$, 0.01, and 0.001.

5.2 Discontinuous Galerkin methods

The results provided in Section 5.1 indicate that *continuous* Galerkin finite element methods are safe to use within the peridynamic framework for problems having smooth solutions but are practically useless for problems with solutions containing jump discontinuities.[§] Problems with smooth solutions can often be handled by classical elasticity models, e.g., local partial differential equation models, so that there may little advantage to using the peridynamic model in that setting. However, problems with discontinuous solutions are exactly the setting in which peridynamics offers an advantage over classical elasticity, so developing effective finite element discretization schemes in this setting is of substantial interest. Because, in the peridynamic setting, the use of continuous finite element methods do not improve upon the classical elastic setting, we turn to *discontinuous* Galerkin methods to see if they can provide such schemes. It is important to note again that such discretizations are *conforming* in the peridynamic setting because that model contains no spatial derivatives. On the other hand, discontinuous Galerkin methods are *nonconforming* in the classical elasticity setting because, in that case, derivatives do appear in the model. For this reason, discontinuous Galerkin methods in the classical elasticity setting require the incorporation of "jump" terms at element boundaries.

5.2.1 Discontinuous piecewise-constant finite elements

We implement the discontinuous piecewise-constant finite element method described in Section 4.2 for the problem having the continuous exact solution given in (3.2). For Table 6 and for the plot on the left of Figure 6, we set the horizon δ proportional to grid size h whereas, for Table 7 and for the plot on the right of Figure 6, we choose δ independent of h. In Tables 8 and 9 and in Figure 7, we provide the analogous results for the discontinuous exact solution given in (3.4).

5.2.2 Discontinuous piecewise-linear finite elements

For the discontinuous piecewise-linear finite element method described in Section 4.3, we only provide results for the case in which the horizon δ is fixed, independent of the grid size h. Results are given in Table 10 and on the left of Figure 8 for the smooth exact solution given in (3.2) and in Table 11 and on the right of Figure 8 for the discontinuous exact solution given in (3.4). For Table 10, the H^1 error is computed as the sum of the element H^1 errors.

5.2.3 Discussion

Based on the results presented in Tables 6–11 and Figures 6–8, we make the following observations.

[§]This is exactly the same as for classical elastic models.

- If the horizon δ is chosen proportional to the grid size h, piecewise-constant approximations fail to converge for both smooth exact solutions and for exact solutions that contain a jump discontinuity.
- On the other hand, if δ is fixed independent of h, piecewise-constant approximations converge for both smooth and discontinuous exact solutions, provided h is sufficiently small relative to δ. Seemingly, one needs $h < \delta$.
- If δ is fixed independent of h, discontinuous piecewise-linear approximations converge at optimal rates for both smooth and discontinuous exact solutions.

From the results, it seems that piecewise-constant approximations are not robust with respect to the relative sizes of the horizon δ and the grid size h. Certainly the apparent restriction that $h < \delta$ can be problematic. On the other hand, it seems that discontinuous piecewise-linear approximations are robust, not only with respect to the relative sizes of δ and h, but also to the smoothness of the solution.

The observation that discontinuous piecewise-linear approximations lead to optimally accurate results for smooth solutions is not surprising, given that they are conforming for the peridynamic model and that they contain as a subspace the continuous piecewise-linear functions, i.e., discontinuous piecewise-linear approximations must be at least as good as continuous piecewise-linear approximations. As was the case for continuous piecewise linear approximations, optimally accurate solutions are obtained for any choice of δ so that again, δ can be interpreted as being a parameter and that can be chosen for convenience.

The observation that discontinuous piecewise-linear approximations lead to optimally accurate results for *discontinuous* solutions illustrates the potential of peridynamic models: one can obtain accurate results for problems with discontinuities for which finite element methods for classical elastic models that involve derivatives have difficulty.

Another interpretation of fact that, for smooth solutions, optimally accurate solutions are obtained for any choice of δ is that, in such a case, δ should not be interpreted as being a material parameter and thus can be chosen for convenience, e.g., to minimize bandwidth or to simplify the coupling of the continuum peridynamic model to atomistic models.

We again note that, at least with respect to the $L^2(\Omega)$ norm, the rates of convergence given in the tables and figures[¶] for the cases for which the horizon δ is chosen independent of the grid size h should be provable. In addition to the coercivity of the bilinear form associated with the variational formulation (4.1), we have that discontinuous finite element spaces are conforming for that variational formulation. For smooth solutions such as those given in (3.2) and (3.3), we should obtain the error estimate (5.1) for discontinuous piecewise-linear approximations and the error estimate

$$\|u - u^h\|_{L^2(\Omega)} \leq C h^{\min\{s,1\}} \|u\|_{H^s(\Omega)}$$

[¶]See Tables 7, 9, 10, and 11 and the plots on the right of Figures 6 and 7 as well as Figure 8.

for discontinuous piecewise-constant approximations. These estimates are entirely consistent with the results in the tables and figures for the smooth solution examples. For the exact solutions with jump discontinuities, i.e., piecewise smooth solutions, we should be able to obtain a "broken-norm" estimate, in case we place a grid point at the points of discontinuity of the exact solution. For example, for the exact solution (3.4), we should be able to obtain the error estimate

$$\|u-u^h\|_{L^2(\Omega)} \leq Ch^r\left(\|u\|_{H^2(\Omega_1)}+\|u\|_{H^2(\Omega_2)}\right)$$

where Ω_1 and Ω_2 denote the two subdomains of Ω on each side of the discontinuity in the exact solution and where $r=1$ and 2 for discontinuous piecewise-constant and discontinuous piecewise-linear approximations, respectively. The rates of convergence given in the appropriate tables and figures are entirely consistent with this estimate.

Table 6: L^2 and L^∞ errors of discontinuous piecewise-constant approximations for the *smooth* exact solution (3.2) and for δ proportional to h.

	$\delta = 2h$		$\delta = 3h$		$\delta = 4h$	
h	L^2 error	L^∞ error	L^2 error	L^∞ error	L^2 error	L^∞ error
2^{-3}	3.56E-2	6.07E-2	2.49E-2	2.02E-2	2.02E-2	4.91E-2
2^{-4}	3.84E-2	5.58E-2	2.42E-2	3.78E-2	1.74E-2	3.17E-2
2^{-5}	4.02E-2	5.61E-2	2.38E-2	3.38E-2	1.59E-2	2.34E-2
2^{-6}	4.12E-2	5.68E-2	2.38E-2	3.30E-2	1.54E-2	2.14E-2
2^{-7}	4.17E-2	5.73E-2	2.39E-2	3.28E-2	1.52E-2	2.09E-2
2^{-8}	4.20E-2	5.76E-2	2.40E-2	3.29E-2	1.51E-2	2.07E-2
2^{-9}	4.22E-2	5.78E-2	2.40E-2	3.29E-2	1.51E-2	2.07E-2
2^{-10}	4.22E-2	5.79E-2	2.40E-2	3.29E-2	1.51E-2	2.07E-2

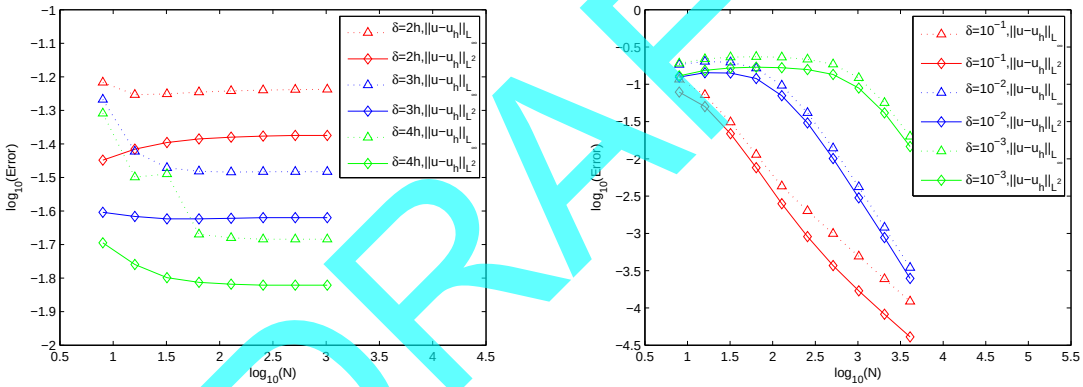

Figure 6: L^2 and L^∞ errors vs. $N = 1/h$ for discontinuous piecewise-constant approximations for the *smooth* exact solution (3.2); left: $\delta = 2h$, $3h$, and $4h$; right: $\delta = 0.1$, 0.01, and 0.001.

Table 7: Errors and convergence rates of discontinuous piecewise-constant approximations for the *smooth* exact solution (3.2) and for δ fixed independent of h.

	$\delta = 0.1$			
	L^2		L^∞	
h	Error	Rate	Error	Rate
2^{-3}	7.85E-2	–	1.16E-1	–
2^{-4}	5.02E-2	0.65	7.21E-2	0.69
2^{-5}	2.17E-2	1.21	3.10E-2	1.22
2^{-6}	7.60E-3	1.51	1.14E-2	1.44
2^{-7}	2.50E-3	1.60	4.30E-3	1.41
2^{-8}	9.05E-4	1.47	2.00E-3	1.10
2^{-9}	3.70E-4	1.29	9.91E-4	1.01
2^{-10}	1.70E-4	1.12	4.92E-4	1.01
2^{-11}	8.24E-5	1.04	2.45E-4	1.01
2^{-12}	4.09E-5	1.01	1.22E-4	1.00

	$\delta = 0.01$			
	L^2		L^∞	
Error	Rate	Error	Rate	
1.25E-1	–	1.84E-1	–	
1.43E-1	–	2.02E-1	–	
1.42E-1	0.01	1.97E-1	0.04	
1.19E-1	0.25	1.65E-1	0.26	
7.02E-2	0.76	9.65E-2	0.77	
3.03E-2	1.47	4.15E-2	1.10	
1.01E-2	1.29	1.39E-2	1.01	
3.00E-3	1.12	4.29E-3	1.01	
8.78E-4	1.04	1.20E-3	1.01	
2.49E-4	1.01	3.47E-4	1.00	

	$\delta = 0.001$			
	L^2		L^∞	
h	Error	Rate	Error	Rate
2^{-3}	1.30E-1	–	1.91E-1	–
2^{-4}	1.54E-1	–	2.16E-1	–
2^{-5}	1.66E-1	–	2.31E-1	–
2^{-6}	1.70E-1	–	2.34E-1	–
2^{-7}	1.67E-1	0.02	2.30E-1	0.02
2^{-8}	1.58E-1	0.08	2.16E-1	0.09
2^{-9}	1.35E-1	0.22	1.86E-1	0.22
2^{-10}	8.90E-2	0.61	1.22E-1	0.61
2^{-11}	4.13E-2	1.11	5.65E-2	1.11
2^{-12}	1.46E-2	1.50	2.00E-2	1.50

Table 8: L^2 and L^∞ errors of discontinuous piecewise-constant approximations for the *discontinuous* exact solution (3.4) and for δ proportional to h.

	$\delta = 2h$		$\delta = 3h$		$\delta = 4h$	
h	L^2 error	L^∞ error	L^2 error	L^∞ error	L^2 error	L^∞ error
2^{-3}	4.14E-2	1.14E-1	3.93E-2	1.09E-1	3.86E-2	1.06E-1
2^{-4}	2.86E-2	7.03E-2	2.41E-2	6.19E-2	2.25E-2	6.00E-2
2^{-5}	2.34E-2	5.08E-2	1.64E-2	3.87E-2	1.36E-2	3.33E-2
2^{-6}	2.19E-2	4.15E-2	1.35E-2	2.82E-2	9.74E-3	2.18E-2
2^{-7}	2.17E-2	3.70E-2	1.26E-2	2.33E-2	8.34E-3	1.66E-2
2^{-8}	2.17E-2	3.48E-2	1.24E-2	2.09E-2	7.91E-3	1.41E-2
2^{-9}	2.17E-2	3.37E-2	1.24E-2	1.97E-2	7.84E-3	1.28E-2
2^{-10}	2.18E-2	3.31E-2	1.24E-2	1.91E-2	7.82E-3	1.22E-2

Table 9: Errors and convergence rates of discontinuous piecewise-constant approximations for the *discontinuous* exact solution (3.4) and for δ fixed independent of h.

	$\delta = 0.1$			
	L^2		L^∞	
h	Error	Rate	Error	Rate
2^{-3}	5.49E-2	–	1.43E-1	–
2^{-4}	3.30E-2	0.73	8.00E-2	0.84
2^{-5}	1.57E-2	1.07	3.79E-2	1.08
2^{-6}	6.80E-3	1.21	1.70E-2	1.16
2^{-7}	3.10E-3	1.13	8.00E-3	1.09
2^{-8}	1.50E-3	1.05	3.90E-3	1.04
2^{-9}	7.32E-4	1.03	2.00E-3	0.96
2^{-10}	3.65E-4	1.01	9.79E-4	1.03
2^{-11}	1.82E-4	1.00	4.89E-4	1.00
2^{-12}	9.10E-5	1.00	2.44E-4	1.00

	$\delta = 0.01$			
	L^2		L^∞	
Error		Rate	Error	Rate
7.43E-2		–	1.79E-1	–
7.64E-2		–	1.52E-1	0.24
7.37E-2		0.01	1.30E-1	0.23
6.21E-2		0.25	1.03E-1	0.34
3.64E-2		0.77	5.93E-2	0.79
1.55E-2		1.23	2.55E-2	1.22
5.20E-3		1.58	9.00E-3	1.50
1.60E-3		1.70	2.90E-3	1.63
4.88E-4		1.71	9.93E-4	1.55
1.61E-4		1.60	3.62E-4	1.46

	$\delta = 0.001$			
	L^2		L^∞	
h	Error	Rate	Error	Rate
2^{-3}	7.65E-2	–	1.83E-1	–
2^{-4}	8.20E-2	–	1.61E-1	0.18
2^{-5}	8.62E-2	–	1.49E-1	0.18
2^{-6}	8.77E-2	–	1.42E-1	0.07
2^{-7}	8.65E-2	0.02	1.35E-1	0.07
2^{-8}	8.13E-2	0.09	1.24E-1	0.12
2^{-9}	7.07E-2	0.20	1.07E-1	0.21
2^{-10}	4.61E-2	0.62	6.95E-2	0.62
2^{-11}	2.11E-2	1.28	3.18E-2	1.13
2^{-12}	7.50E-3	1.49	1.13E-2	1.49

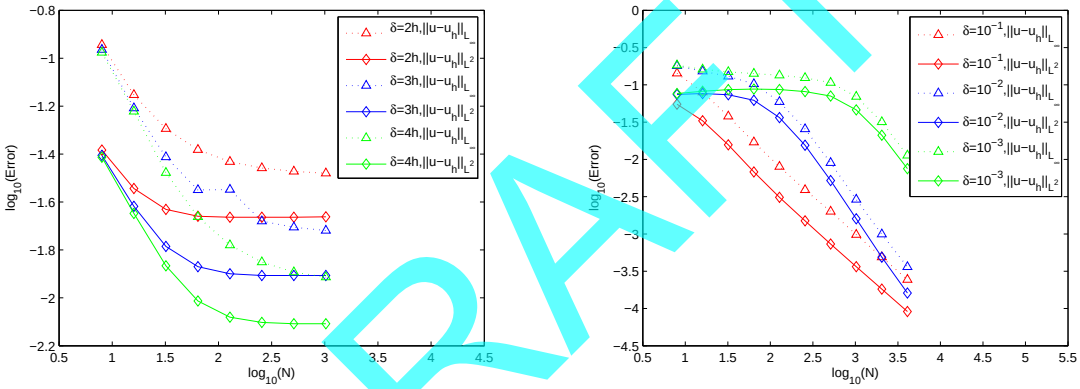

Figure 7: L^2 and L^∞ errors vs. $N = 1/h$ for discontinuous piecewise-constant approximations for the *discontinuous* exact solution (3.4); left: $\delta = 2h$, $3h$, and $4h$; right: $\delta = 0.1$, 0.01, and 0.001.

Table 10: Errors and convergence rates of discontinuous piecewise-linear approximations for the *smooth* exact solution (3.2) and for $\delta = 0.001$.

	L^2		L^∞		H^1	
h	Error	Rate	Error	Rate	Error	Rate
2^{-3}	2.50E-3	–	3.90E-3	–	6.25E-2	–
2^{-4}	6.58E-4	1.93	9.71E-4	2.01	3.38E-2	0.89
2^{-5}	1.71E-4	1.94	2.44E-4	1.99	1.75E-2	0.95
2^{-6}	4.41E-5	1.96	6.13E-5	1.99	8.90E-3	0.98
2^{-7}	1.11E-5	1.99	1.53E-5	2.00	4.50E-3	0.98
2^{-8}	2.80E-6	1.99	3.85E-6	1.99	2.20E-3	1.03
2^{-9}	6.82E-7	2.04	9.44E-7	2.03	1.10E-3	1.00
2^{-10}	1.70E-7	2.00	2.38E-7	1.99	5.63E-4	0.97

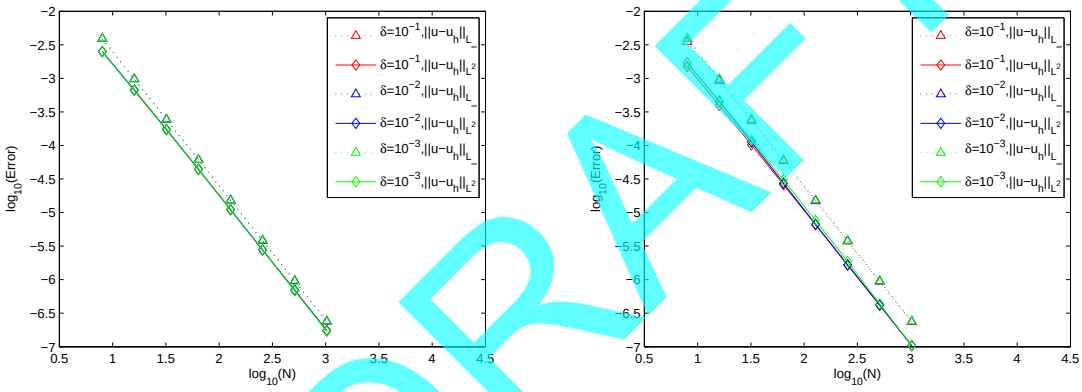

Figure 8: L^2 and L^∞ errors vs. $N = 1/h$ for discontinuous piecewise-linear approximations for $\delta = 0.1$, 0.01, and 0.001; left: *smooth* exact solution (3.2); right: *discontinuous* exact solution (3.4).

Table 11: Errors and convergence rates of discontinuous piecewise-linear approximations for the *discontinuous* exact solution (3.4) and for $\delta = 0.001$.

	L^2		L^∞	
h	Error	Rate	Error	Rate
2^{-3}	1.70E-03	1.77	3.90E-03	2.01
2^{-4}	4.65E-04	1.87	9.71E-04	2.01
2^{-5}	1.20E-04	1.95	2.44E-04	2.00
2^{-6}	3.06E-05	1.98	6.10E-05	2.00
2^{-7}	7.58E-06	2.01	1.52E-05	2.00
2^{-8}	1.86E-06	2.03	3.81E-06	2.00
2^{-9}	4.37E-07	2.09	9.45E-07	2.01
2^{-10}	1.04E-07	2.06	2.38E-07	1.99

5.3 A Hybrid Continuous-Discontinuous Galerkin Method

From Sections 5.1 and 5.2, it is clear, for the discontinuous exact solution (3.4), that discontinuous piecewise-linear finite element approximations results in the greater accuracy compared to either the continuous piecewise-linear and the discontinuous piecewise-constant approximations; see the summary in Table 12 for the exact solution given in (3.4). However, for the same number of finite element intervals, the discontinuous piecewise-linear method has greater complexity than the other two; again see Table 12. Which approach is better, with respect to accuracy per unit cost, between methods having greater accuracy and complexity and those having lesser accuracy and complexity depends on the number of space dimensions and the method selected for solving the linear systems.

Table 12: For the exact solution (3.4), a comparison of the L^2 rates of convergence and matrix properties for continuous-linear (CL), discontinuous-constant (DC), and discontinuous-linear (DL) finite element approximations for $h=1/(N+1)$ and $\delta=Mh$, where N and M are positive integers.

	CL	DC	DL
L^2 errors	$O(N^{-1/2})$	$O(N^{-1})$	$O(N^{-2})$
number of unknowns	N	$N+1$	$2N+2$
dimensions of matrix	$N\times N$	$(N+1)\times(N+1)$	$(2N+2)\times(2N+2)$
half bandwidth of matrix	$M+1$	M	$2M+1$

In Section 5.1, we saw that that for continuous exact solutions such as those given in (3.2) and (3.3), continuous piecewise-linear approximations are optimally accurate. This observation offers the possibility of using such approximations for smooth parts of a solution having jump discontinuities and using discontinuous piecewise-linear approximations only in a "small" neighborhood of the jump discontinuity. In this way, we hope to preserve the high accuracy of the discontinuous piecewise-linear approximations for solutions having jump discontinuities, but with a complexity very near that of continuous piecewise-linear approximations. We test this idea for the *discontinuous* exact solution (3.4); the results are given in Table 11 and Figure 9. Discontinuous basis functions are used only in two intervals. We see that even though we use continuous approximations almost everywhere, the hybrid approximation results in optimally accurate rates of convergence. Note that this is achieved without any need for grid refinement.

Of course, for the exact solution given in (3.4), we know exactly where to switch from continuous to discontinuous approximating functions. In practice, we would not know beforehand where discontinuities, e.g., cracks, occur so that one would have to implement some type of method to detect the formation of discontinuities and then adaptively choose the type of basis functions used to match the location of the discontinuities. This is all quite possible within the peridynamics framework.

Table 13: Errors and convergence rates of hybrid discontinuous/continuous piecewise-linear approximations for the *discontinuous* exact solution (3.4) and for $\delta = 0.1$.

	L^2		L^∞	
h	Error	Rate	Error	Rate
2^{-3}	1.50E-03	1.74	3.50E-03	1.97
2^{-4}	3.94E-04	1.93	9.12E-04	1.94
2^{-5}	1.02E-04	1.95	2.34E-04	1.97
2^{-6}	2.60E-05	1.97	5.91E-05	1.98
2^{-7}	6.57E-06	1.99	1.49E-05	1.99
2^{-8}	1.65E-06	1.99	3.73E-06	1.99
2^{-9}	4.14E-07	2.00	9.36E-07	2.00
2^{-10}	1.04E-07	2.00	2.34E-07	2.00

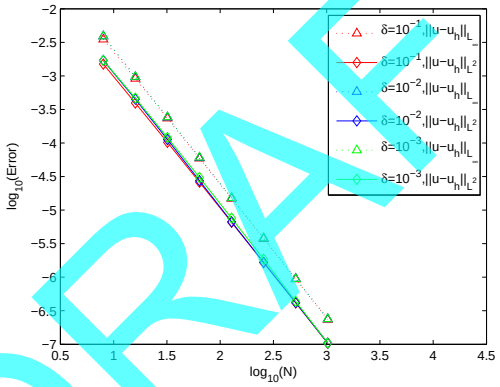

Figure 9: L^2 and L^∞ errors vs. $N = 1/h$ for hybrid discontinuous/continuous piecewise-linear approximations for the *discontinuous* exact solution (3.4) with $\delta = 0.1$, 0.01, and 0.001.

6 Concluding Remarks

We have shown that finite element discretizations of the peridynamic model for materials has the potential of producing accurate solutions, even for discontinuous solutions. In particular, discontinuous piecewise-linear approximations are apparently robustly optimally accurate with respect to choices for the model parameter, i.e., the horizon δ, and the smoothness of the solution.

However, we need to repeat the caveat given above: we have considered the special situation in which a grid point is located exactly at the point of discontinuity of the exact solution. In general, this is difficult to accomplish, especially in two- and three dimensions where discontinuities across curves and surfaces may occur. Table 14 and Figure 10 give an indication of what can happen if one does not place a grid point at the location of the discontinuity of the solution. We emphasize, however, that unlike for discontinuous piecewise linear finite element approximations, continuous finite element approximations yields results similar to those in Table 14 and Figure 10 *even if a grid point is placed at a point of discontinuity*; see Table 5 and Figure 5. Similar behavior can be expected if one uses continuous finite element approximations for classical elastic models.

Current and future work will address means for recovering the accuracy and robustness of discontinuous piecewise-linear discretizations of peridynamics models; certainly adaptive strategies can play an important role in this regard. Extending the algorithms and implementations to two and three dimensions and to nonlinear problems is also of interest as is the use of higher-order discontinuous piecewise polynomials. Many issues will arise in such studies, including proper choices for quadrature rules. Certainly, a rigorous numerical analysis of discontinuous finite element discretizations is also highly desirable to have in hand.

Table 14: Errors and convergence rates of discontinuous piecewise-linear approximations for the *discontinuous* exact solution (3.4) for the case in which there is no grid point located at the point of discontinuity of the solution.

	$\delta = 0.1$				$\delta = 0.01$			
	L^2		L^∞		L^2		L^∞	
h	Error	Rate	Error	Rate	Error	Rate	Error	Rate
3^{-2}	2.31E-2	–	1.24E-1	–	2.38E-2	–	1.25E-1	–
3^{-3}	1.34E-2	0.50	1.23E-1	0.01	1.35E-2	0.52	1.23E-1	0.01
3^{-4}	0.77E-2	0.50	1.23E-1	0	0.77E-2	0.51	1.23E-1	0
3^{-5}	0.45E-2	0.49	1.23E-1	0	0.45E-2	0.49	1.23E-1	0
3^{-6}	0.26E-2	0.50	1.23E-1	0	0.26E-2	0.49	1.23E-1	0
3^{-7}	0.15E-2	0.50	1.23E-1	0	0.15E-2	0.50	1.23E-1	0

	$\delta = 0.001$			
	L^2		L^∞	
h	Error	Rate	Error	Rate
3^{-2}	2.42E-2	–	1.26E-1	–
3^{-3}	1.43E-2	0.48	1.24E-1	0.02
3^{-4}	0.80E-2	0.53	1.23E-1	0
3^{-5}	0.46E-2	0.50	1.23E-1	0
3^{-6}	0.26E-2	0.52	1.23E-1	0
3^{-7}	0.15E-2	0.50	1.23E-1	0

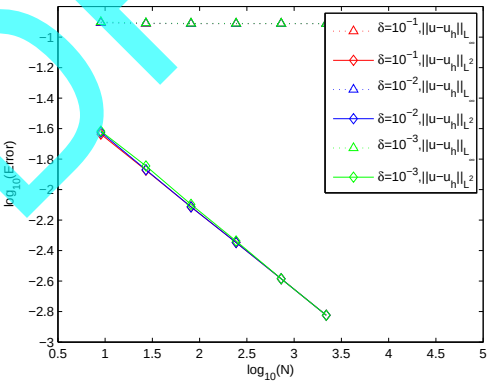

Figure 10: L^2 and L^∞ errors vs. $N = 1/h$ for discontinuous piecewise-linear approximations for the *discontinuous* exact solution (3.4) for the case in which there is no grid point located at the point of discontinuity of the solution.

A Well-Posedness of the Variational Problem

In this section, we prove the existence and uniqueness of the solution of (2.15), or more precisely, of its variational formulation (4.1). Similar and more extensive results are obtained in [10] and also in [17].

We assume that boundary condition data $g(x)=0$. Define the bilinear form $A(\cdot,\cdot): S\times S\to\mathbb{R}^1$and the continuous linear functional on S by

$$A(u,v)=\int_\alpha^\beta\int_{x-\delta}^{x+\delta} v(x)\frac{u(x)-u(x')}{|x-x'|}\mathrm{d}x'\mathrm{d}x$$

and

$$F(v)=\delta^2\int_\alpha^\beta b(x)v(x)\mathrm{d}x,$$

respectively. We have that

$$A(u,v)=\Big(\int_\alpha^{\alpha+\delta}\int_{x-\delta}^{\alpha}+\int_\alpha^\beta\int_{\max(\alpha,x-\delta)}^{\min(\beta,x+\delta)}+\int_{\beta-\delta}^{\beta}\int_{\beta}^{x+\delta}\Big)v(x)\frac{u(x)-u(x')}{|x-x'|}\mathrm{d}x'\mathrm{d}x.$$

Because $g(x)=0$, we have that $u(x')=0$ for $x'\in[\alpha-\delta,\alpha]\cup[\beta,\beta+\delta]$ so that

$$A(u,v)=A_1(u,v)+A_2(u,v)+A_3(u,v),$$

where

$$\begin{cases} A_1(u,v)=\displaystyle\int_\alpha^{\alpha+\delta}\int_{x-\delta}^{\alpha} v(x)\frac{u(x)}{x-x'}\mathrm{d}x'\mathrm{d}x \\ A_2(u,v)=\displaystyle\int_\alpha^\beta\int_{\max(\alpha,x-\delta)}^{\min(\beta,x+\delta)} v(x)\frac{u(x)-u(x')}{|x-x'|}\mathrm{d}x'\mathrm{d}x \\ A_3(u,v)=\displaystyle\int_{\beta-\delta}^{\beta}\int_{\beta}^{x+\delta} v(x)\frac{u(x)}{x-x'}\mathrm{d}x'\mathrm{d}x. \end{cases}$$

Because the integration region of $A_2(u,v)$ is symmetric along $x=x'$, we have that

$$\begin{aligned} A_2(u,v) &= \int_\alpha^\beta\int_{\max(\alpha,x-\delta)}^{\min(\beta,x+\delta)}\frac{u(x)-u(x')}{|x-x'|}v(x)\mathrm{d}x'\mathrm{d}x \\ &= \int_\alpha^\beta\int_{\max(\alpha,x'-\delta)}^{\min(\beta,x'+\delta)}\frac{u(x)-u(x')}{|x-x'|}v(x)\mathrm{d}x\mathrm{d}x' \\ &= -\int_\alpha^\beta\int_{\max(\alpha,x-\delta)}^{\min(\beta,x+\delta)}\frac{u(x)-u(x')}{|x-x'|}v(x')\mathrm{d}x'\mathrm{d}x \end{aligned}$$

so that

$$A_2(u,v)=\frac{1}{2}\int_\alpha^\beta\int_{\max(\alpha,x-\delta)}^{\min(\beta,x+\delta)}\big(v(x)-v(x')\big)\frac{u(x)-u(x')}{|x-x'|}\mathrm{d}x'\mathrm{d}x.$$

We now show that $A(\cdot,\cdot)$ defines an inner product. First, note that

$$\begin{aligned} A_1(u,u) &= \int_{\alpha}^{\alpha+\delta} u^2(x) \int_{x-\delta}^{\alpha} \frac{1}{x-x'} \mathrm{d}x' \mathrm{d}x \\ &= \int_{\alpha}^{\alpha+\delta} u^2(x) \ln \frac{\delta}{x-\alpha} \mathrm{d}x = -\delta \int_0^1 u^2(\alpha+\delta y) \ln y \mathrm{d}y \geq 0 \end{aligned}$$

so that, because $\ln y < 0$ for $y \in (0,1)$ and $\int_0^1 \ln y \mathrm{d}y = -1$, we have that, if we assume u is bounded,

$$0 \leq A_1(u,u) < \infty.$$

Moreover,

$$A_1(u,u) = 0 \quad \text{implies that} \quad u(x) = 0 \quad \text{for a.e. } x \in [\alpha, \alpha+\delta].$$

Similarly, we have that

$$0 \leq A_3(u,u) < \infty \qquad \text{and} \qquad A_3(u,u) = 0 \quad \text{implies that} \quad u(x) = 0 \quad \text{for a.e. } x \in [\alpha, \alpha+\delta].$$

We have that

$$A_2(u,u) = \frac{1}{2} \int_{\alpha}^{\beta} \int_{\max(\alpha, x-\delta)}^{\min(\beta, x+\delta)} \frac{\left(u(x)-u(x')\right)^2}{|x-x'|} \mathrm{d}x' \mathrm{d}x \geq 0.$$

Moreover, for all $x, x' \in [\alpha, \beta]$, $A_2(u,u) = 0$ implies that $u(x) - u(x') = 0$ so that $u(x) =$ constant for $x \in [\alpha, \beta]$. We then have that $A(u,u) \geq 0$ and

$$A(u,u) = 0 \iff A_1(u,u) = A_2(u,u) = A_3(u,u) = 0 \iff u(x) = 0, \quad \text{for } x \in [\alpha, \beta].$$

Also, it is obvious that

$$A(u,v) = A(v,u) \qquad \text{and} \qquad A(\alpha u + \beta v, w) = \alpha A(u,w) + \beta A(v,w).$$

Collecting the above results, we have that $A(u,v)$ defines an inner product that induces the norm

$$\begin{aligned} |||u|||^2 = A(u,u) \quad &= \int_{\alpha}^{\alpha+\delta} \int_{x-\delta}^{\alpha} \frac{u^2(x)}{x-x'} \mathrm{d}x' \mathrm{d}x \\ &+ \int_{\alpha}^{\beta} \int_{\max(\alpha, x-\delta)}^{\min(\beta, x+\delta)} \frac{(u(x)-u(x'))}{|x-x'|} \mathrm{d}x' u(x) \mathrm{d}x \\ &+ \int_{\beta-\delta}^{\beta} \int_{\beta}^{x+\delta} \frac{u^2(x)}{x-x'} \mathrm{d}x' \mathrm{d}x. \end{aligned} \tag{A.1}$$

Let

$$|||b|||_* = \sup_{v \in S_0, v \neq 0} \frac{\delta^2 \int_{\alpha}^{\beta} v(x) b(x) dx}{|||v|||}$$

and define the "dual" space $S_0^* = \{b(x) : |||b(x)|||_* < \infty\}$. The, the variational problem (4.1) has the following form: given $b(x) \in S_0^*$, seek $u \in S$, such that

$$A(u,v) = F(v) \qquad \forall v \in S_0$$

Because $A(\cdot,\cdot)$ defines an inner product on S, it is continuous and coercive on that space. Then, if we assume that the functional $F(v)$ is continuous, the Lax-Milgram theorem can be applied to show that our variational problem has a unique solution and, moreover, those solutions satisfy

$$|||u||| \leq |||b|||_*.$$

It can also then be shown that finite element discretizations of the variational formulation results in approximations that are optimally accurate with respect to the induced norm $|||\cdot|||$. In [10], this norm is related to standard Sobolev norms, and in particular to the L^2 norm.

References

[1] B. ALTAN, Uniqueness of initial-boundary value problems in nonlocal elasticity; *Int. J. Solids Struct.* **25** 1989, 1271-1278.

[2] B. ALTAN, Uniqueness in nonlocal thermoelasticity; *J. Thermal Stress.* **14** 1991, 121-128.

[3] Z. BAZANT AND M. JIRASEK, Nonlocal integral formulations of plasticity and damage: Survey and progress; *J. Eng. Mech.* **128** 2002, 1119-1149.

[4] F. BOBARU AND S. SILLING, Peridynamic 3D problems of nanofiber networks and carbon nanotube-reinforced composites; in *Materials and Design: Proc. Inter. Conf. Numerical Methods in Industrial Forming Processes*, American Institute of Physics, 2004, 1565-1570.

[5] F. BOBARU, S. SILLING, AND H. JIANG, Peridynamic fracture and damage modeling of membranes and nanofiber networks; in *Proc. XI Int. Conf. Fracture*, Turin, 2005, 5748:1-6.

[6] F. BOBARU, M. YANG, L. ALVES, S. SILLING, E. ASKARI, AND J. XU, Convergence, adaptive refinement, and scaling in 1D peridynamics; *Inter. J. Numer. Meth. Engrg.* **77** 2009, 852-877.

[7] Y. CHEN, J. LEE, AND A. ESKANDARIAN, Atomistic viewpoint of the applicability of microcontinuum theories; *Int. J. Solids Struct* **41** 2004, 2085-2097.

[8] C. CHEN AND T. SHIH, *Finite Element Methods for Integrodifferential Equations*, World Scientific, Singapore, 1998.

[9] K. DAYAL AND K. BHATTACHARYA, Kinetics of phase transformations in the peridynamic formulation of continuum mechanics; submitted to *J. Mech. Phys. Solids.*

[10] Q. DU AND K. ZHOU, Mathematical analysis for the peridynamic nonlocal continuum theory; submitted.

[11] E. EMMRICH AND O. WECKNER, The peridynamic equation of motion in non-local elasticity theory; in *Proc. III European Conference on Computational Mechanics Solids, Structures and Coupled Problems in Engineering*, Lisbon, 2006.

[12] E. EMMRICH AND O. WECKNER, Analysis and numerical approximation of an integrodifferential equation modelling non-local effects in linear elasticity; *Math. Mech. Solids* **12** 2007, 363-384.

[13] E. EMMRICH AND O. WECKNER, On the well-posedness of the linear peridynamic model and its convergence towards the Navier equation of linear elasticity; *Commun. Math. Sci.* **5** 2007, 851-864.

[14] E. EMMRICH AND O. WECKNER, The peridynamic equation and its spatial discretization; *Math. Model. Anal.* **12** 2007, 17-27.
[15] W. GERSTLE AND N. SAU, Peridynamic modeling of concrete structures; in *Proc. 5th Int. Conf. Fract. Mech. Concr. Struct.* L. Li et al. (eds.), Ia-FRAMCOS, 2004 **2**, 949-956.
[16] W. GERSTLE, N. SAU, AND S. SILLING, Peridynamic modeling of plain and reinforced concrete structures; in *SMiRT18: 18th Int. Conf. Struct. Mech. React. Technol.*, Beijing, 2005.
[17] M. GUNZBURGER AND R. LEHOUCQ, A nonlocal vector calculus with application to nonlocal boundary value problems; Part 1: The Scalar Case; submitted, 2009
[18] E. KRONER, Elasticity theory of materials with long range forces; *Inter. J. Solids Struct.* **3** 1967, 731-742.
[19] I. KUNIN, *Elastic Media with Microstructure*, Vol. I and II, Springer, Berlin, 1982/83.
[20] V. LAKSHMIKANTHAM AND M. RAO, *Theory of Integro-differential Equations*, Gordon and Breach, Lausanne, 1995.
[21] Y. LEI, M. FRISWELL, AND S. ADHIKARI, A Galerkin method for distributed systems with non-local damping; *Inter. J. Solids Struct.* **42** 2005, published online first, DOI: 10.1016/j.ijsolstr.2005.06.058.
[22] R. MACEKA AND S. SILLING, Peridynamics via finite element analysis; *Finite Elem. Anal. Design* **4** 2007, 1169-1178.
[23] A. PISANO AND P. FUSCHI, Closed form solution for a nonlocal elastic bar in tension; *Inter. J. Solids Struct.* **40** 2003, 13-23.
[24] C. POLIZZOTTO, Nonlocal elasticity and related variational principles; *Inter. J. Solids Struct.* **38** 2001, 7359-7380.
[25] D. ROGULA, *Nonlocal Theory of Material Media*, Springer, Berlin, 1982.
[26] S. SILLING, Reformulation of elasticity theory for discontinuities and long-range forces; *J. Mech. Phys. Solids* **48** 2000, 175-209.
[27] S. SILLING, Dynamic fracture modeling with a meshfree peridynamic code; in *Computational Fluid and Solid Mechanics*, K. Bathe (ed.), Elsevier, Amsterdam, 2003, 641-644.
[28] S. SILLING AND E. ASKARI, Peridynamic modeling of impact damage; in *PVP-Vol. 489* F. Moody (ed.), ASME, New York, 2004, 197-205.
[29] S. SILLING AND E. ASKARI, A meshfree method based on the peridynamic model of solid mechanics; *Comput. Struct* **83** 2005, 1526-1535.
[30] S. SILLING AND F. BOBARU, Peridynamic modeling of membranes and fibers; *Int. J. Nonlinear Mech.* **40** 2005, 395-409.
[31] S. SILLING, M. ZIMMERMANN, AND R. ABEYARATNE, Deformation of a peridynamic bar; *J. Elasticity* **73** 2003, 173-190.
[32] J. WANG AND R. DHALIWAL, Uniqueness in generalized nonlocal thermoelasticity; *J. Thermal Stresses* **16** 1993, 71-77.
[33] J. WANG AND R. DHALIWAL, On some theorems in the nonlocal theory of micropolar elasticity; *Int. J. Solids Struct.* **30** 1993, 1331-1338.
[34] O. WECKNER AND R. ABEYARATNE, The effect of long-range forces on the dynamics of a bar; *J. Mech. Phys. Solids* **53** 2005, 705-728.
[35] O. WECKNER AND E. EMMRICH, Numerical simulation of the dynamics of a nonlocal, inhomogeneous, infinite bar; *J. Comp. Appl. Mech.* **6** 2005, 311-319.
[36] O. WECKNER AND E. EMMRICH, Energy conserving spatial discretisation methods for the peridynamic equation of motion in non-local elasticity theory; *Preprint 25-2005*, Institute of Mathematics, TU Berlin, 2005.
[37] M. ZIMMERMANN, *A Continuum Theory with Long-Range Forces for Solids*, Ph.D. Thesis, De-

partment of Mechanical Engineering, Massachusetts Institute of Technology, 2005.